

RESEARCH PROJECT NOISE - SC01

D1.5d Rotorcraft noise modelling guidance



Disclaimer



This study has been carried out for the European Union Aviation Safety Agency by an external organization and expresses the opinion of the organization undertaking the study. It is provided for information purposes only and the views expressed in the study have not been adopted, endorsed or in any way approved by the European Union Aviation Safety Agency. Consequently it should not be relied upon as a statement, as any form of warranty, representation, undertaking, contractual, or other commitment binding in law upon the European Union Aviation Safety Agency.

Ownership of all copyright and other intellectual property rights in this material including any documentation, data and technical information, remains vested to the European Union Aviation Safety Agency. All logo, copyrights, trademarks, and registered trademarks that may be contained within are the property of their respective owners.

Reproduction of this study, in whole or in part, is permitted under the condition that the full body of this Disclaimer remains clearly and visibly affixed at all times with such reproduced part.

REPORT NUMBER: D1.5d

REPORT CLASSIFICATION: UNCLASSIFIED

DATE: 31 January 2024

KNOWLEDGE AREA(S): Rotorcraft Technology; Aeroacoustic and Experimental Aerodynamics; Aircraft noise prediction

DESCRIPTOR(S): Helicopter noise; NORAH; Validation

CUSTOMER: EASA

CONTRACT NUMBER: EASA.2020.FC.06

OWNER: European Union Aviation Safety Agency

DISTRIBUTION: Limited

CLASSIFICATION OF TITLE: UNCLASSIFIED

Author(s):

H. Olsen, M. Tuinstra, N. van Oosten

APPROVED BY: AUTHOR

REVIEWER

MANAGING DEPARTMENT

Choose an item.

DATE: Click or tap to enter a date.

RESEARCH PROJECT NOISE - SC03

D1.5d Rotorcraft noise modelling guidance

Royal Netherlands Aerospace Centre (NLR)

Royal NLR operates as an unaffiliated research centre, working with its partners towards a better world tomorrow. As part of that, Royal NLR offers innovative solutions and technical expertise, creating a strong competitive position for the commercial sector. It is an organisation that works to achieve sustainable, safe, efficient and effective aerospace operations.

Anthony Fokkerweg 2 | 1059 CM Amsterdam | + 31 88 511 3113 | + 31 88 511 3210 | info@nlr.nl | www.nlr.org

A. Scope and purpose of the guidance

Rotorcraft noise emission is strongly dependent on flight conditions and varies heavily with emission angles. In order to obtain high fidelity noise prediction a dedicated method is required to model rotorcraft noise. Land-use planning methods in Europe that were developed for fixed-wing aircraft are described in ECAC Doc 29¹. A complementary method – Noise of Rotorcraft Assessed by a Hemisphere-approach – is detailed hereafter to model rotorcraft noise, suited to support strategic noise mapping activities.

The guidance targets both *practitioners* and *modellers*. As the guidance matures it might be opted to create separate volumes for both as is the case for ECAC Doc 29.

A.1 Overview and rationale of the method

The rotorcraft noise modelling method allows the prediction of noise levels for standard rotorcraft operations targeting the most common types within the European helicopter fleet. The method starts by considering the noise levels at an observer location \mathbf{x} , the latter being a function of the time dependent rotorcraft location $\mathbf{y}(t)$ and centre frequency f_c :

	$L_o(f_c, \mathbf{x}, \mathbf{y}(t)) = L(f_c, \varphi, \theta, V, \gamma) + \Delta L_p$	(1)
--	---	------------

The observer noise level is decomposed in a source term L and a scaling factor to account for atmospheric propagation ΔL_p . The latter term comprises those effects relating to spherical spreading, atmospheric attenuation and ground absorption.

For an accurate source description of a given rotorcraft type, the method relies on sets of measured noise hemispheres, covering a broad range of lateral and polar emission angles and the relevant conditions in the flight envelope. Noise hemispheres provide a source description, given in one-third octave bands, from which SEL, EPNdB, $L_{A,max}$ and other noise metrics can be derived.

A hemisphere approach is followed to describe the rotorcraft noise source. Next-generation rotorcraft noise models show a consensus that this allows to adequately capture the complex and highly directive nature of helicopter noise. Hemispheres are defined as function of azimuth φ and polar angle θ , binned in intervals of 10 degrees. This approach differs from the Noise Power Distance methods for fixed wing aircraft noise, allowing (i) separate handling of the modelling of source and noise propagation and (ii) the detailed description of emission characteristics of helicopter noise.

To allow representation of a large portion of the European helicopter fleet based on a limited set of helicopter noise data, helicopter types with assumed similar noise characteristics are clustered together within a single class. The parameters considered to determine the classes are summarized in Table 1, where the premise is that noise hindrance caused by a specific rotorcraft type relates directly to these parameters. The resulting helicopter classes are specified in Table 2, where only the classes comprising more than a single helicopter are given. In the source term $L_{i,j}$, i and j are, respectively, the helicopter class index and time dependent flight condition index.

Table 1 Parameter overview of collected configuration data and noise level information

Parameter	Explanation
Maximum Take-Off Weight [kg]	
Main rotor number of blades	
Main rotor direction of rotation (viewed from above)	CW = Clockwise, CCW = Counter-Clockwise, Co-ax = Coaxial rotors, Intermesh = intermeshing rotors
Tail rotor number of blades	
Tail rotor position	L = Left, R = Right, in fin = Fan-in-fin, NOTAR = No Tail Rotor
Engine type	P = Piston, T = Turbine
Engine number	
ICAO noise level, take-off [EPNdB]	for Chapter 8 helicopters
ICAO noise level, overflight [EPNdB]	for Chapter 8 helicopters
ICAO noise level, approach [EPNdB]	for Chapter 8 helicopters
ICAO noise level, overflight [dBA]	for Chapter 11 helicopters

Table 2 Helicopter classes containing more than one helicopter type, types within square brackets denote geometrically mirrored configurations

Helicopter class	ATD	Included helicopter types
Agusta A109	A109	A109, B105, B427, B429, BK17, EC45
AgustaWestland AW189	A189	A189, A149, [EC75]
AS332 Super Puma	AS32	AS32, AS3B
AS350 Ecureuil	AS50	AS50, ALO2, ALO3, LAMA, PSW4
AS355 Ecureuil 2	AS55	AS55, MI2
AS365 Dauphin 2	AS65	AS65, EC55
Bell 206 JetRanger	B06	B06, B06T, B47T, H12T, R66
Bell 212	B212	B212, B222, B230
Bell 412	B412	B412, B430, S76

Helicopter class	ATD	Included helicopter types
Bell UH-1 Iroquois	UH1	UH1, HUCO
Dynali H2	DYH2	DYH2, [ULTS], plus a number of homebuilts like Dynali H3, Rotorsmart HeliSmart, [Ultrasport 331]
EC120 Colibri	EC20	EC20, EC30, GAZL
EC135	EC35	EC35, EC145T2
EC225 Super Puma	EC25	EC25, MI8
Enstrom 480	EN48	EN48, S330
Famà Kiss 209	K209	K209, B150, [ES11], [EXEJ]
PZL-Swidnik W-3 Sokol	W3	W3, PUMA
Robinson 22	R22	R22, CH7, V500, [A600], [BABY], [DRAG], [EXEC], [SCOR], plus a number of homebuilts like EliSport CH-77 Ranabot, Cicaré CH-7T Spirit Tandem, BHR Mustang F260N, BHR Mustang F290, Hungarocopter HC-01, Italian Rotors T22, BHR Fandango F360, [LCA Helicopter LH212]
Robinson 44	R44	R44, B47G, B47J, ELTO, UH12
Schweizer 300	H269	H269, BRB2, EN28, [ZA6]

A.2 Input data generation

A.2.1 Operational data

To perform noise maps, an overview of the type of rotorcrafts, a list of rotorcraft operations and their and their associated flight tracks are a prerequisite.

Radar track data is the most readily available source of information of actual (rotorcraft) flight paths and the recommendations on how to deal with this data source as outlined in ECAC Doc.29, vol.2, section 3.2.1 remain pertinent. The limitation described in the first paragraph of this subsection forces the user adapt the vertical flight profiles to the noise database. It is the role of the noise practitioner to define modelled trajectories which best match the radar data.

A.2.2 Rotorcraft mapping and substitution

A clustering into classes is adopted to model the European rotorcraft fleet. In case a rotorcraft type is modelled for which a noise database was established for another helicopter within its class, or when no noise database is established for its class at all, this needs further consideration.

To allow variations in noise levels within a class, an offset of hemisphere levels based on the difference (ΔL_{EPNL}) between registered certification levels⁹ of the class reference and the helicopter type under consideration is applied. The noise level for a helicopter type in class i at flight condition j and emission angles θ and φ is then given by

$L(f_c, \varphi, \theta, V, \gamma) = \hat{L}_i(f_c, \varphi, \theta, V, \gamma) + \Delta L_{EPNL}$	(2)
---	------------

where $\hat{L}_i(f_c, \varphi, \theta, V, \gamma)$ is defined by eq. 8. The correction is applied to the overall hemisphere noise levels based on the difference in certification noise levels. For 'Chapter 8' certified helicopters, climb, level and descent conditions shall be corrected based, respectively, on the take-off, overflight and approach certification levels.

Classes with more than one helicopter type are given in Table 2. Several helicopter type indicators are within brackets, e.g. [A600] in the R22 class, to indicate that the main/tail rotor configuration is mirrored with respect to the class reference. In this case the hemisphere azimuth angle has to be mirrored, hence the \pm symbol in eq. 2.

In case no hemisphere set is available for a given helicopter class, a dedicated hemisphere set is recommended to be acquired by carrying out noise measurements. An intermediate solution is to temporarily group the helicopter type with a class for which a noise database is available. In this case certification noise levels are decisive and should be lower than or within the range of the target helicopter class. In case no certification noise levels are available or multiple classes can be selected based on this criterion, helicopter weight becomes the governing parameter. The class with the best matching weight that is still lower than the helicopter type considered is selected. ΔL_{EPNL} is set to zero to ensure a conservative estimate of noise levels.

A.2.3 Weather conditions

Weather conditions (atmospheric pressure, temperature, wind speed and relative humidity) have an influence on the sound propagation through the atmosphere, affecting atmospheric attenuation, ground absorption and sound refraction. Atmospheric attenuation is influenced the strongest, whereas for ground absorption it mainly influences the frequencies at which constructive or destructive interference occurs.

Refraction – the curving of sound rays – is not covered by the present method. Modelling refraction would require a detailed knowledge on the atmosphere temperature and velocity profiles.

A.2.4 Topographical data

When there is a need to account for variations in terrain elevation relative to the airport reference elevation, methods described in section A.4.4 and A.4.5 may be applied

The method operates on a geometrical model consisting of a set of connected ground and obstacles surfaces. Any sound propagation path is considered in a vertical plane through the receiver and a point source.

In the plane of the path, the topography may be described by a set of discrete points $(x_k, z_k); k \in \{1, \dots, n\}$. This terrain profile is represented by a mean plane by linear regression. The mean plane is used for calculation of ground effect and diffraction from topography.

A.3 Source model

A.3.1 Flight conditions

The rotorcraft noise source is described by a set of hemispheres covering a range of flight conditions relevant to noise emission. The flight condition is characterised by both airspeed and rate of flight angle of the rotorcraft.

Figure 2 shows a diagram with the impulsive noise boundaries as function of airspeed and Rate of Climb/Descent for the UH-1 helicopter. Two areas can be identified: (i) an area related to Blade Vortex Interaction (BVI) that occurs mainly for descending flight; (ii) another area associated with high-speed impulsive noise, which occurs when the rotorcraft is in fast forward flight. Although the exact location of their boundaries will vary depending on rotorcraft type, this diagram is applicable to any rotorcraft. An example of the impact on noise emission is shown in Figure 3, presenting maximum A-weighted sound pressure levels as function of climb- and airspeed for the R22 helicopter. A difference of up to 10 dB in noise levels is observed over the covered flight envelope. A second observation is that the noise levels vary little (generally within 1 dB) as function of rate of climb.

Figures 2 and 3 enable to conclude that, for descents, helicopter noise will vary strongly depending on airspeed and descent angle. These variations should be captured in the hemisphere data set that make up the source model. Hemispheres shall be available at descent angle intervals of minimum 3 degrees and 4 different velocities are recommended to cover the operational range. The climb region is sufficiently covered by considering a number of climb angles, e.g., 3, 6 and 9 degrees, at the best rate of climb speed (V_y) or a speed typically used in take-off procedures. It is recommended to further: (i) include the maximum climb angle as stated in the aircraft flight manual; (ii) keep level flight conditions at 90% of the speed at level flight for maximum continuous power (V_H) and +10 kts (or V_H whichever is the smallest), -15 kts and -30 kts increments on $0.9 V_H$.

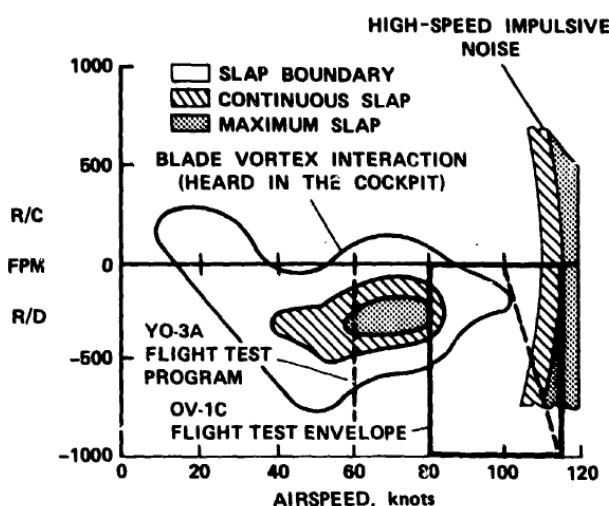


Figure 1 Impulsive noise boundaries for UH-1 series helicopter, from Schmitz et. al¹⁸

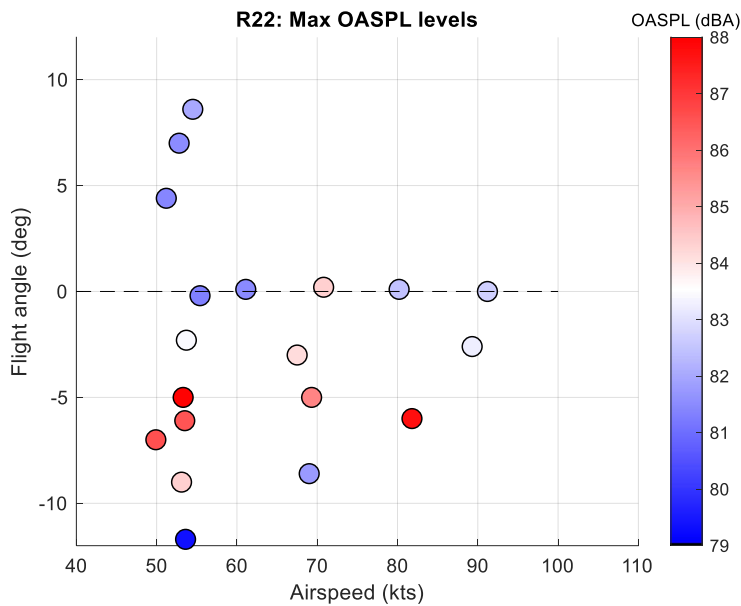


Figure 2 R22 maximum A-weighted sound pressure level at centre microphone, from NORAH1 database.

The hemispheres can be interpolated between the flight conditions to allow for flight conditions which are not in the database.

The interpolation method first requires a normalization of the flight path angle γ and airspeed V . Then if the required hemisphere flight condition is within the convex hull of the database flight conditions distance scaled triangulation interpolation can be applied, as indicated by Figure 3a. If the required database point is outside of the convex hull, nearest neighbour interpolation should be applied. Nearest neighbour interpolation uses the hemisphere with the flight conditions closest to the required flight condition is the best estimate for the hemisphere at the required flight condition.

The interpolation can be applied using the following rules:

1. Select the hemispheres for the appropriate helicopter type in the NORAH database.
2. Normalize the NORAH database flight angles and airspeeds with the minimal and maximal flight condition values in the database. Multiply γ_j with the flight condition scaling factor $F_{fc}=2$, which was empirically determined to give minimum interpolation error.

	$\bar{\gamma}_j = F_{fc} \frac{\gamma_j}{\gamma_{max} - \gamma_{min}}$	(3)
	$\bar{V}_j = \frac{V_j}{V_{max} - V_{min}}$	(4)

3. Normalize the required flight angle and the airspeed with the minimal and maximal flight conditions values in the database. Multiply γ with the flight condition scaling factor $F_{fc}=2$.

	$\bar{\gamma} = F_{fc} * \frac{\gamma}{\gamma_{max} - \gamma_{min}}$	(5)
--	--	------------

	$\bar{V} = \frac{V}{V_{max} - V_{min}}$	(6)
--	---	-----

4. Calculate the Delaunay triangulation for the database flight conditions $\bar{\gamma}_j$ and \bar{V}_j , see Figure 3. This can also be done using a lookup table, as the triangulation does not change for a given helicopter database.
5. If the required flight condition $(\bar{\gamma}, \bar{V})$ is enveloped by a triangle, interpolation is possible :

Apply the triangulation interpolation:

- a. Find the distance between database points to the required normalized flight conditions:

	$\delta_j = \sqrt{(\bar{\gamma} - \bar{\gamma}_j)^2 + (\bar{V} - \bar{V}_j)^2}$	(7)
--	---	-----

- b. Calculate the required hemisphere by interpolating the values of the three hemispheres scaled with the distance to the required flight conditions:

	$\hat{L}_i(f_c, \varphi, \theta, V, \gamma) = 10 \log_{10} \left(\frac{\sum_{j \in T_k} \frac{10^{\frac{\tilde{L}_{ij}(f_c, \varphi, \theta)}{10}}}{\delta_j}}{\sum_{j \in T_k} \frac{1}{\delta_j}} \right)$	(8)
--	---	-----

, where T_k is the triangle enveloping flight conditions $\bar{V}, \bar{\gamma}$

6. If the flight conditions is not enveloped by a triangle interpolation, is not possible.

Apply the nearest neighbour interpolation:

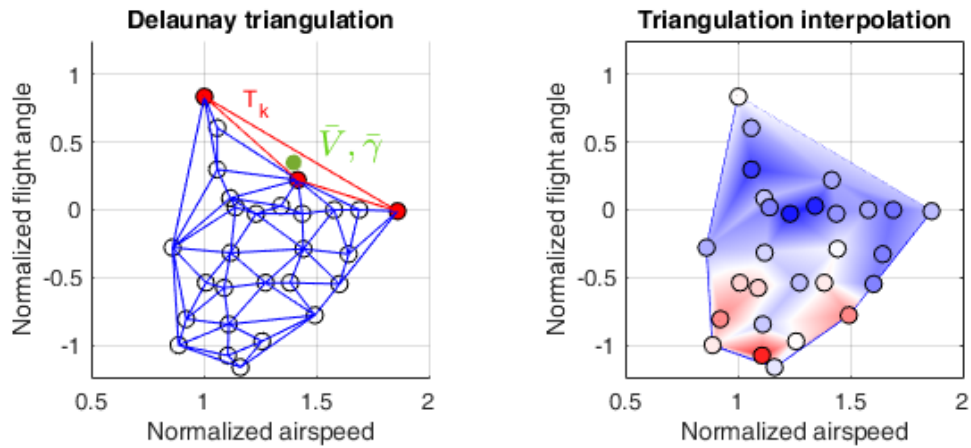
- a. Calculate the distance from the required flight condition to all database points j , per eq. 12.
- b. Find the database point with the flight conditions closest to the required flight conditions

	$\underset{j}{\operatorname{argmin}}\{\delta_j\} = \delta(\gamma_l, V_l)$	(9)
--	---	-----

where l is the index δ_j achieves its minimum value

- c. Adopt this nearest hemisphere as the required hemisphere.

	$\hat{L}_i(f_c, \varphi, \theta, V, \gamma) = \tilde{L}_{i,l}(f_c, \varphi, \theta)$	(10)
--	--	------



(a)

(b)

Figure 3 (a) Delaunay triangulation applied to normalized flight conditions of NORAH EC120 helicopter hemispheres, as example Triangle T_k is indicated (b) Distance scaled triangulation interpolation.

A.3.2 Noise hemispheres

As a prerequisite to the method, the rotorcraft noise source needs to be described via a hemisphere (see Appendix A for hemisphere data format). This follows a state-of-the-art approach as hemispheres provide an adequate manner to describe the complex and highly directive nature of rotorcraft noise phenomena. Notwithstanding this fact, it is noteworthy that noise measurements for the purpose of hemisphere derivation should be performed with great care, and generally follow the guidelines given in ICAO Annex 16.

Hemisphere noise levels are defined at a fixed reference distance of 60 metres and include effects of atmospheric absorption under ICAO certification atmospheric reference conditions ($p_a = 101325 \text{ Pa}$, $T = 298.15 \text{ K}$ and $h_{rel} = 70\%$) This distance matches that used for the frequency extrapolation method outlined in ICAO Doc 9501¹⁵. The latter is used to reconstruct masked one-third octave bands levels above 2 kHz, assuming a flat spectrum (equal energy) following the last good band. Hemispheres are composed of one-third octave bands, for frequencies between 10Hz (10th band) to 10kHz (40th band).

Hemispheres are defined as function of azimuth θ and polar angle φ , binned in intervals of 10 degrees. The emission angles are related to Cartesian coordinates in the aircraft body axis system as follows:

$$\begin{aligned}
 x &= r_h \cos \theta \\
 y &= r_h \sin \theta \sin \varphi \\
 z &= r_h \sin \theta \cos \varphi
 \end{aligned}
 \tag{11}$$

in which $-90^\circ \leq \varphi \leq 90^\circ$ and $0^\circ \leq \theta \leq 180^\circ$.

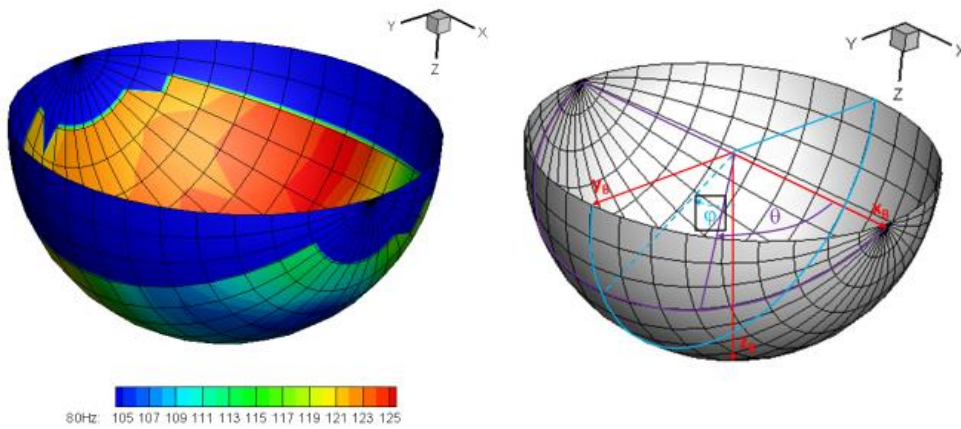


Figure 4 Example of a noise hemisphere (left), based on measurements of a R22 helicopter, 80Hz 1/3 octave band frequency, given in aircraft body axis system(right)

Negative and positive azimuth angles correspond, respectively, to port and starboard of the rotorcraft. For polar angles $\theta < 90^\circ$ noise emits in the forward direction and for $\theta > 90^\circ$ in the rearward direction of the rotorcraft (see figure 2).

The example hemisphere shows that its surface is not filled entirely with noise data. For both practical reasons and data quality-related issues, hemisphere data is required to cover at least the following emission angles:

$-60^\circ \leq \varphi \leq 60^\circ$ $\theta_{t1} \leq \theta \leq \theta_{t2}$	(12)
---	-------------

where θ_{t1} and θ_{t2} correspond to the polar angles at 10 dB down time instance. Measurement of higher lateral angles or polar angles approaching $0^\circ/180^\circ$ is possible but require complex measurement setups^{16,17}.

To obtain source levels from stored hemispheres, a bilinear interpolation is applied as follows

$\tilde{L}_{i,j}(f_c, \varphi, \theta) = 10 \log_{10} \left(\left[\frac{\varphi^{m+1} - \varphi}{\Delta\varphi} \quad \frac{\varphi - \varphi^m}{\Delta\varphi} \right] \begin{bmatrix} 10^{\frac{L_h(f_c)_{i,j}^{m,n}}{10}} & 10^{\frac{L_h(f_c)_{i,j}^{m,n+1}}{10}} \\ 10^{\frac{L_h(f_c)_{i,j}^{m+1,n}}{10}} & 10^{\frac{L_h(f_c)_{i,j}^{m+1,n+1}}{10}} \end{bmatrix} \left[\frac{\theta^{n+1} - \theta}{\Delta\theta} \right] \right)$	(13)
---	-------------

in which m and n are the azimuth and polar index respectively, with $\varphi^m < \varphi < \varphi^{m+1}$ and $\theta^n < \theta < \theta^{n+1}$. When exceeding the range for which data is available, constant value extrapolation should be applied from the nearest filled data bin, filling any gaps in the hemispheres. The nearest bin is given by the subset of indices for which $\rho_{m,n}$ is minimized:

$\underset{m,n}{\operatorname{argmin}} \{ \rho_{m,n} \}$	(14)
--	-------------

In this $\varrho_{m,n}$ is the absolute angle between a bin and target value φ, θ , defined by:

	$\rho_{m,n} = \cos^{-1}(x(\varphi, \theta) \cdot x_{m,n})$	(15)
--	--	-------------

The vectors \mathbf{x} and $\mathbf{x}_{m,n}$ are given by eq. 11, with $r_h=1$. In case there are multiple closest bins, the energetic average of the closest bins is taken.

A.3.3 Flight path construction

For flight path construction ECAC Doc 29, Vol.1, section 4.8 should be followed. The vertical profile of each rotorcraft should be defined using a sequence of procedural steps based on the flight conditions for which noise hemispheres are available and their respective durations. Rotorcraft pitch attitude is included implicitly in the hemispheres and shall not specified explicitly.

As mentioned in A.2.1 Radar track data is the most readily available source of information of actual (rotorcraft) flight paths. For noise calculation, next to position, the helicopter velocity, bank-angle and climb angle are needed, which may be derived from radar track data. Based on the velocity and climb angle the appropriate hemisphere maybe selected. The bank angle allows to accurately model the emission pattern.

Radar track data includes a level of noise with a typical accuracy of around 5 to 10 m. Furthermore, time registration is often rounded to full seconds given an error of maximum 0.5 s. For typical rotorcraft speeds this results in a positioning error of 10 m to 20 m. To derive velocity, climb- and bank angles, it is essential to apply smoothing to the radar data to filter out unrealistic oscillations. This can be achieved by spline interpolation, which has the added benefit that the user may generate position data at higher sampling time Δt_s (e.g. every second).

At each timestep t of the refined and smoothed track the ground velocity is determined as

	$V_g = \frac{\Delta S}{\Delta t_s} = \frac{\sqrt{(\Delta X^2 + \Delta Y^2)}}{\Delta t_s}$	(16)
--	---	-------------

and

	$V_A = \frac{\sqrt{(\Delta X^2 + \Delta Y^2 + \Delta Z^2)}}{\Delta t_s}$	(17)
--	--	-------------

based on finite difference around t . The resulting velocity is defined with respect to ground surface, which neglects wind.

The bank angle may be defined based on the velocity, together with radius of curvature of the track. The latter may be determined as

	$K = \frac{\Delta\Theta}{\Delta S}$	(18)
--	-------------------------------------	-------------

in which $\Delta\Theta$ is the change in heading Θ at timestep t obtained by finite differences. The heading Θ follows from the two-argument tangent

	$\Theta = \text{atan}_2 \frac{\Delta X}{\Delta Y}$	(19)
--	--	-------------

at each timestep t . The bank angle Φ may now be derived on the basis of

	$\Phi = \text{atan} \left(\frac{KV_g^2}{g} \right)$	(20)
--	--	-------------

The path angle is given by.

	$\gamma = \text{acos} \frac{\Delta Z}{\Delta S}$	(21)
--	--	-------------

The interpolation method described in section A.3.1 allows to obtain the source description for the flight conditions that follow from radar data. Note that the velocity V_A should be used to find the best matching hemisphere, not V_g .

For specific phases of a flight such as, turns, hover, taxiing

A.3.4 Turns

To model the noise levels in turns level-flight hemispheres are used that are tilted using the bank angle (eq. 20). The level flight hemisphere with the closest matching velocity should be employed.

The following approach is followed to include turns in the noise modelling:

1. For level turns: the level-flight hemisphere with the speed that best reflects the speed during the turn should be chosen and tilted using the bank angle.
2. For turns during take-off: the take-off hemisphere should be chosen with the speed that best reflects the speed during the turn and tilted using the bank angle.
3. For turns during descent: the level-flight hemisphere should be chosen with the speed that best reflects the speed during the turn and tilted using the bank angle.

The interpolation method described in section A.3.1 interpolates between flight conditions and therefore for a given velocity and flight path angle, automatically the right source description is obtained.

A.3.5 Hover, idle and taxi

In case noise measurements and source descriptions for hover and idle are available these should be employed.

Otherwise, the approaches listed (summarized in Table 3) below with descending priority, may be employed.

Approach 1:

Measure noise for in-ground hover, out of ground hover, full-rpm idle and reduced-rpm idle for the full directivity (polar angle θ) following the CAEP guidance for in-ground hover.

Approach 2:

1. Measure noise for in-ground hover for the full directivity (θ) following the CAEP guidance for in-ground hover.
2. Measure noise for out of ground hover, full-rpm idle and reduced-rpm idle for the 0-degree direction.
3. Derive noise hemisphere for in-ground hover by assuming constant directivity in φ .
4. Derive noise hemispheres for out of ground hover, full-rpm idle, and reduced-rpm idle using the directivity pattern of in-ground hover and the offset for the 0-degree direction between in-ground hover and out of ground hover, full-rpm idle, and reduced-rpm idle, respectively and assuming constant directivity in φ .

Approach 3:

1. Measure noise for in-ground hover for the full directivity (θ) following the CAEP guidance for in-ground hover.
2. Derive noise hemisphere for in-ground hover by assuming constant directivity in φ .
3. Derive noise hemispheres for out of ground hover, full rpm idle, and reduced-rpm idle using the directivity pattern of in-ground hover and add offset of 12 dB* to derive out of ground hover from the in-ground hover disk, -12 dB* to derive reduced-rpm idle from in-ground hover disk, and -2.5 dB* to derive full-rpm idle from out of ground hover and assuming constant directivity in φ .

Table 3 Summary of approaches to derive LA-levels (dB) for in-ground hover (HIGE), out of ground hover (HOGE), reduced-rpm idle (Gr. idle), and full-rpm idle (Fl. idle).

	Approach 1	Approach 2	Approach 3
HIGE	Measure $LA_{HIGE}(\theta)$	Measure $LA_{HIGE}(\theta)$	Measure $LA_{HIGE}(\theta)$
HOGE	Measure $LA_{HOGE}(\theta)$	Measure $LA_{HOGE}(0^\circ)$ $\Delta LA_{HOGE}(0^\circ) = LA_{HOGE}(0^\circ) - LA_{HIGE}(0^\circ)$ $LA_{HOGE}(\theta) = LA_{HIGE}(\theta) + \Delta LA_{HOGE}(0^\circ)$	$LA_{HOGE}(\theta) = LA_{HIGE}(\theta) + 12 \text{ dB}^*$
Gr. idle	Measure $LA_{Gr.idle}(\theta)$	Measure $LA_{Gr.idle}(0^\circ)$ $\Delta LA_{Gr.idle}(0^\circ) = LA_{Gr.idle}(0^\circ) - LA_{HIGE}(0^\circ)$ $LA_{Gr.idle}(\theta) = LA_{HIGE}(\theta) + \Delta LA_{Gr.idle}(0^\circ)$	$LA_{Gr.idle}(\theta) = LA_{HIGE}(\theta) - 12 \text{ dB}^*$
Fl. idle	Measure $LA_{FL.idle}(\theta)$	Measure $LA_{FL.idle}(0^\circ)$ $\Delta LA_{FL.idle}(0^\circ) = LA_{FL.idle}(0^\circ) - LA_{HIGE}(0^\circ)$	$LA_{FL.idle}(\theta) = LA_{HIGE}(\theta) - 2.5 \text{ dB}^*$

$$LA_{FL, idle}(\theta) = LA_{HIGE}(\theta) + \Delta LA_{FL, idle}(0^\circ)$$

***Note:** *the indicated offsets were derived from measurements with inverted microphones on ground plates. Recently EMPA found that these values may not be valid for other microphone setups (e.g., 4m height over hard or soft ground). Further investigation is required to validate these values or propose updated ones.*

In the case that no hover data is available, as a first approximation the noise data from 2 side-line microphones during level flight with the lowest available speed may be used. Appropriate propagation effects shall be applied in accordance with the ICAO Annex 16 integrated method and maintaining the measured θ values, to correct the data to the hover geometry (circle with 150m radius). Constant directivity in φ is to be assumed.

To include taxiing for helicopters with and without wheels into the noise calculation the measured and derived hemispheres for in-ground hover and full-rpm idle respectively should be employed.

A.4 Propagation model

A.4.1 Spherical spreading, emitted and recorded time

A time delay is experienced between emission and reception of noise related to the time required for a sound wave to reach an observer. The relation between recorded time t_r and emitted time t_e is given by

$$t_r = t_e + \frac{r}{c} \quad (22)$$

where c is the speed of sound and r is the distance between rotorcraft and observer. At ICAO reference conditions ($p_a = 101325$ Pa, $T = 298.15$ K and $h_{rel} = 70\%$) the speed of sound is $c = 346.1$ m/s. To evaluate time integrated metrics, e.g. SEL or EPNL, it is required to express the predicted noise levels as a function of recorded time.

The total noise attenuation due to propagation

$$\Delta L_p = \Delta L_s + \Delta L_a + \Delta L_g + \Delta L_d \quad (23)$$

is governed by shielding and diffraction (ΔL_d), ground attenuation (ΔL_g), atmospheric attenuation (ΔL_a) and spherical spreading losses

$$\Delta L_s = -20 \log_{10} \frac{r}{r_h} \quad (24)$$

where $r_h = 60$ m is the hemisphere reference distance. The contributions for ground attenuation and atmospheric attenuation will be addressed below.

A.4.2 Atmospheric attenuation

An unimpeded propagating plane acoustic wave is still attenuated due to atmospheric absorption. This is caused by losses due to shear viscosity, thermal effects and molecular relaxation. These losses vary with temperature, pressure and in case of molecular (nitrogen and oxygen) relaxation losses, with humidity. They are also frequency dependent. A propagating plane wave attenuated by the atmosphere can be written as

$$p(t, s) = p_0 e^{-as} e^{i(\omega t - ks)} \quad (25)$$

where p is the pressure amplitude at a distance s , p_0 is the initial wave amplitude and a is the atmospheric attenuation in Nepers per metre. This can be expressed in decibels by

$$\begin{aligned} \Delta L_{a,t}(f) &= -20 \log_{10} \frac{|p(t, s)|}{p_0} = -20 \log_{10} e^{-as} \\ &= -\alpha(f)(r - r_h) \end{aligned} \quad (26)$$

where α ($=20/\ln 10 \cdot a$) is the attenuation in dB/m.

The method described in SAE ARP5534¹⁹ is followed to obtain α at ICAO reference conditions. The pure-tone mid-band attenuation coefficient given by

$$\alpha = 8.686f^2 \left\{ 1.8556 \cdot 10^{-11} + 6.6928 \cdot 10^{-6} \cdot \frac{f_{rO}}{f_{rO}^2 + f^2} + 1.3415 \cdot 10^{-6} \cdot \frac{f_{rN}}{f_{rN}^2 + f^2} \right\} \quad (27)$$

where f is the pure-tone frequency of sound in Hz and the variables $f_{rN} = 75692$ Hz and $f_{rO} = 630.7$ Hz represent the vibrational relaxation frequencies of oxygen and nitrogen respectively. Eq. 27 gives the attenuation in dB/m for a pure-tone frequency. To infer the atmospheric attenuation for a one-third octave band the SAE method by Rickley et al.²⁰ is applied (see Table 4 and Figure 5).

Table 4 Tabulated values of one-third octave band atmospheric attenuation per km propagation distance

f_c , Hz	$\Delta L_a/km$, dB	f_c , Hz	$\Delta L_a/km$, dB
10	0.0	400	2.3
12.5	0.0	500	3.1
16	0.0	630	4.1
20	0.0	800	5.2
25	0.0	1000	6.3
31.5	0.0	1250	7.5
40	0.0	1600	8.9
50	0.0	2000	10.6
63	0.1	2500	13.0
80	0.1	3150	16.6
100	0.2	4000	22.5
125	0.3	5000	31.0
160	0.5	6300	44.9
200	0.7	8000	67.6
250	1.1	10000	101.0
315	1.6		

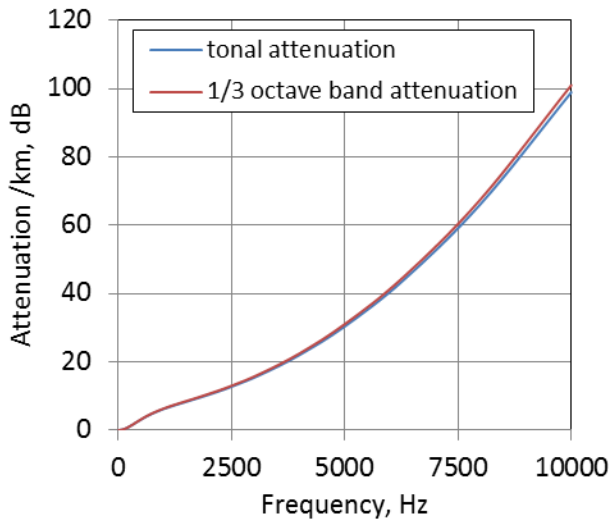


Figure 5 Tonal and one-third octave band atmospheric attenuation per km propagation distance

A.4.3 Ground absorption

The solution^{21,22,23} for a point source above an impedance surface is given by:

$$p(x) = \frac{e^{ikr_1}}{r_1} + Q \frac{e^{ikr_2}}{r_2} \quad (28)$$

where p is the complex pressure amplitude, k the wavenumber, Q is the spherical reflection coefficient and r_1 and r_2 are the direct and reflected path length respectively. Assuming Q is approximately constant within a one-third octave band, the ground attenuation as function of centre frequency is given by²⁴

$$\Delta L_g = 10 \log \left\{ 1 + \frac{r_1^2}{r_2^2} |Q|^2 + 2 \frac{r_1}{r_2} |Q| I \right\} \quad (29)$$

in which

$$I = \frac{\sin\left(\frac{0.727f_c \Delta R}{c}\right)}{\frac{0.727f_c \Delta R}{c}} \cos\left(\frac{6.325f_c \Delta R}{c} + \psi\right) \quad (30)$$

accounts for the interference patterns that occurs within a band. ΔR is the path length difference between the direct and reflected ray, c the speed of sound and ψ the argument of the spherical reflection coefficient. Eq. 30 shows that in the high frequency limit, I tends to zero and eq. 29 reduces to a summation of two uncorrelated noise sources.

The spherical reflection coefficient Q is given by

$$Q = R_p + (1 - R_p)F(d) \quad (31)$$

where

$$R_p = \frac{Z_s \cos \xi - 1}{Z_s \cos \xi + 1} \quad (32)$$

is the planar wave reflection coefficient. In the latter expression, Z_s is the surface impedance and ξ the angle of incidence of the incoming acoustic wave (0° corresponding to normal incidence). In eq.(16), F is a boundary loss factor, defined by

$$F(d) = 1 + id\sqrt{\pi}e^{-d^2} \operatorname{erfc}(-id) \quad (33)$$

which is a function of numerical distance

$$d = \frac{(1+i)}{2} \sqrt{kr_2} \left(\frac{1}{Z_s} + \cos \xi \right) \quad (34)$$

The complementary error function for complex arguments (erfc) is evaluated by numerical approximations^{25,26} (see Appendix B).

The surface impedance Z_s is modelled by a single parameter model by Delaney and Bazley²⁷, which strikes a good balance between ease of use and accuracy. The surface is assumed locally reacting so that the surface impedance Z_s is equal to the specific normalized impedance of the ground medium. The surface impedance is then given by

$$Z_s = \left\{ 1 + 0.0511 \left(\frac{f}{\sigma} \right)^{-0.754} \right\} + i \left\{ 0.0768 \left(\frac{f}{\sigma} \right)^{-0.732} \right\} \quad (35)$$

The variables f and σ are, respectively, the frequency and the flow resistivity of the material. The recommended surface types are either concrete ($\sigma = 65 \cdot 10^6 \text{ Pa} \cdot \text{s}/\text{m}^2$) for city areas or grass field ($\sigma = 200 \cdot 10^3 \text{ Pa} \cdot \text{s}/\text{m}^2$) for rural areas. Other surface types are described in Table 5 Table of flow resistivity data of common ground type classes (from CNOSSOS EU method)^[29]

Description	Class	(kPa·s/m ²)
Very soft (snow or moss-like)	A	12.5

Soft forest floor (short, dense heather-like or thick moss)	B	31.5
Uncompacted, loose ground (turf, grass, loose soil)	C	80
Normal uncompacted ground (forest floors, pasture field)	D	200
Compacted field and gravel (compacted lawns, park area)	E	500
Compacted dense ground (gravel road, car park)	F	2000
Hard surfaces (most normal asphalt, concrete)	G	20 000
Very hard and dense surfaces (dense asphalt, concrete, water)	H	200 000

and may be used when applicable.

Table 5 Table of flow resistivity data of common ground type classes (from CNOSSOS EU method)^[29]

Description	Class	(kPa·s/m ²)
Very soft (snow or moss-like)	A	12.5
Soft forest floor (short, dense heather-like or thick moss)	B	31.5
Uncompacted, loose ground (turf, grass, loose soil)	C	80
Normal uncompacted ground (forest floors, pasture field)	D	200
Compacted field and gravel (compacted lawns, park area)	E	500
Compacted dense ground (gravel road, car park)	F	2000
Hard surfaces (most normal asphalt, concrete)	G	20 000
Very hard and dense surfaces (dense asphalt, concrete, water)	H	200 000

A.4.4 Ground absorption for varying topography

The method described in section A.4.3 assumes flat terrain of one particular type. If the terrain height and surface is varying the effective ground absorption may be different from the case of horizontal ground with even flow resistivity. To account for this, the real vertical cross-section between the source and the receiver shall be represented by the corresponding *Mean Ground Plane* (MGP). This can be calculated by least square regression of the polyline of the straight segments that form the terrain profile.

$$z = ax + b \quad (36)$$

where

$$a = \frac{3(2A - B(x_n + x_1))}{(x_n - x_1)^3} \quad (37)$$

$$b = \frac{2(x_n^3 - x_1^3)}{(x_n - x_1)^4} B - \frac{3(x_n + x_1)}{(x_n - x_1)^3} A \quad (38)$$

$$A = \frac{2}{3} \sum_{k=1}^{n-1} a_k (x_{k+1}^3 - x_k^3) + \sum_{k=1}^{n-1} b_k (x_{k+1}^2 - x_k^2) \quad (39)$$

$$B = \sum_{k=1}^{n-1} a_k (x_{k+1}^2 - x_k^2) + 2 \sum_{k=1}^{n-1} b_k (x_{k+1} - x_k) \quad (40)$$

The ground absorption is calculated according to the description in E.3, using an angle of incidence relative to the MGP. In some cases, the application of MGP can lead to negative height for the source or receiver. This shall be avoided by limiting minimum source and receiver height to 0.1 meter above the MGP.

The attenuation due to the ground effect is mainly the result of the interference between the reflected sound and the sound that is propagated directly from the source to the receiver. It is physically linked to the acoustic absorption of the ground above which the sound wave is propagated. However, it is also significantly dependent on atmospheric conditions during propagation, as ray bending modifies the height of the path above the ground and makes the ground effects more or less significant.

The ground effect is calculated according to equations for ground reflections, described in section A.4.3. Here a flat ground is assumed at the mean plane. To take into account the actual relief of the land along a propagation path in the best possible way, the notion of 'equivalent height' is introduced, which substitutes real heights in the ground effect equations.

We will assume the following notation. Real heights above the ground are noted by h and equivalent heights are to be noted by z . The equivalent heights are obtained from the mean ground plane between the source and the receiver. This replaces the actual ground with a fictitious plane representing the mean profile of the land (see Figure 6). Instructions on the method for calculating the mean plane are given above.

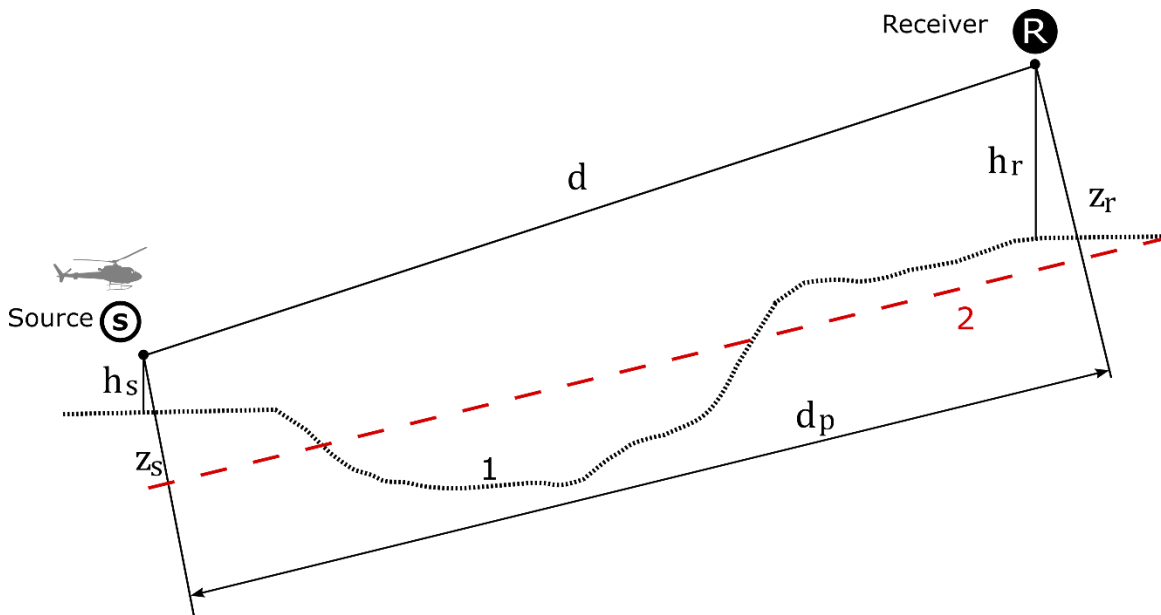


Figure 6 Equivalent heights in relation to the ground

- 1: Actual relief
- 2: Mean plane

The acoustic absorption properties of the ground are mainly linked to its porosity. Compact ground is generally reflective and porous ground is absorbent. Table 5 Table of flow resistivity data of common ground type classes (from CNOSSOS EU method)^[29]

Description	Class	(kPa·s/m ²)
Very soft (snow or moss-like)	A	12.5
Soft forest floor (short, dense heather-like or thick moss)	B	31.5
Uncompacted, loose ground (turf, grass, loose soil)	C	80
Normal uncompacted ground (forest floors, pasture field)	D	200
Compacted field and gravel (compacted lawns, park area)	E	500
Compacted dense ground (gravel road, car park)	F	2000
Hard surfaces (most normal asphalt, concrete)	G	20 000
Very hard and dense surfaces (dense asphalt, concrete, water)	H	200 000

gives the different types of ground classes.

If the type of ground is not the same across the terrain profile, the flow resistivity should be averaged by the logarithm.

$$\bar{\sigma} = 10 \left[\frac{1}{\sum d_i} \sum_{i=1}^n (d_i * \log(\sigma_i)) \right] \quad (41)$$

Where d_i is the length of each ground segment (see for example Figure 7), and σ_i is the flow resistivity of the segment surface.

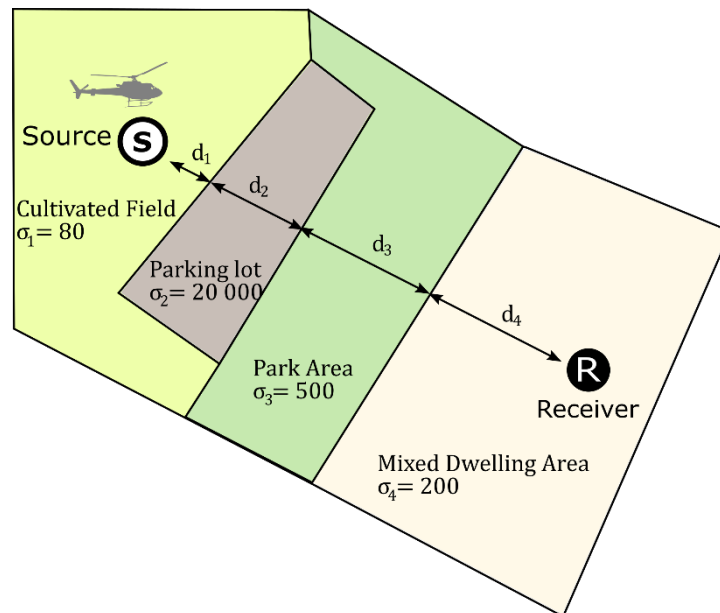


Figure 7 Determination of mean average flow resistivity over a propagation path.

A.4.5 Screening effects from buildings and topography

Screening by building- and topography edges trigger the use of algorithms for diffraction effects. This screening effect shall be calculated by use of the *Path Length Difference* (see Appendix C for definition of noise paths) as the dominant parameter. When an obstacle interferes with the line of sight between a source and a receiver, this is the difference between the shortest path above/around the obstacle and the direct source-to-receiver line (as if the obstacle was not there). As a general rule, the diffraction should be studied at the top of each obstacle located on the propagation path. If the path passes ‘high enough’ over the diffraction edge, $\Delta L_d = 0$ can be set and a direct line of sight is calculated, in particular by evaluating ΔL_g (see section A.4.3 and A.4.4).

For each frequency band centre frequency, the path difference δ is compared with the quantity $-\lambda / 20$, where λ is the acoustic wavelength. If the path difference δ is less than $-\lambda / 20$, there is no need to calculate ΔL_d for

the frequency band considered. In other words, $\Delta L_d = 0$ in this case. Otherwise, ΔL_d is calculated as described in the remainder of this part. This rule applies in all weather conditions, for both single and multiple diffraction.

NOTE: When, for a given frequency band, a calculation is made according to the procedure described in this section, the ground effect ΔL_g is included and should not be evaluated separately by the methods described in section A.4.3 or A.4.4.

The equations proposed here are used to process the diffraction on thin screens, thick screens, buildings, earth berms (natural or artificial), and by the edges of embankments, cuttings and viaducts.

Figure 8 illustrates the general method and principles of calculation of the attenuation due to diffraction. This method is based on breaking down the propagation path into two parts: the 'source side' path, located between the source and the diffraction point, and the 'receiver side' path, located between the diffraction point and the receiver.

The following are calculated:

- a ground effect, source side, $\Delta L_{g,s}$
- a ground effect, receiver side, $\Delta L_{g,r}$
- and three diffractions:
 - between the source S and the receiver R : $\Delta L_{d,s}$
 - between the image source S' and R : $\Delta L_{d,s'}$
 - between S and the image receiver R' : $\Delta L_{d,r'}$.

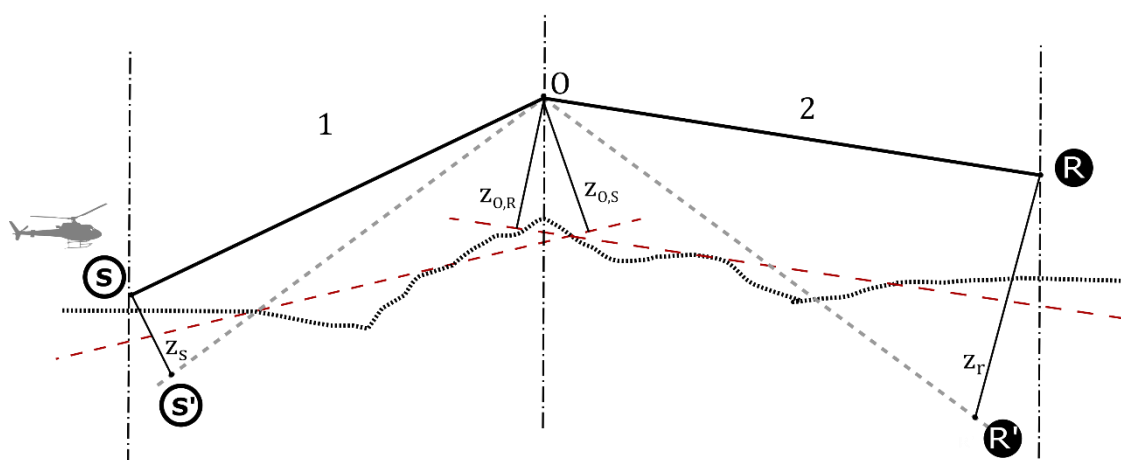


Figure 8 Geometry of a calculation of the attenuation due to diffraction

- 1: Source side**
- 2: Receiver side**

where

S is the source;

R is the receiver;

S' is the image source in relation to the mean ground plane source side;

R' is the image receiver in relation to the mean ground plane receiver side;

O is the diffraction point;

z_s is the equivalent height of the source S in relation to the mean plane source side;

$z_{o,s}$ is the equivalent height of the diffraction point O in relation to the mean ground plane source side;

z_r is the equivalent height of the receiver R in relation to the mean plane receiver side;

$z_{o,r}$ is the equivalent height of the diffraction point O in relation to the mean ground plane receiver side.

The irregularity of the ground between the source and the diffraction point, and between the diffraction point and the receiver, is taken into account by means of equivalent heights calculated in relation to the mean ground plane, source side first and receiver side second (two mean ground planes), according to the method described in section A.4.4.

For pure diffraction, with no ground effects, the attenuation is given by:

$$\Delta L_d = \begin{cases} 10 C_h \cdot \log_{10} \left(3 + \frac{40}{\lambda} C'' \delta \right) & \text{if } \frac{40}{\lambda} C'' \delta \geq -2 \\ 0 & \text{otherwise} \end{cases} \quad (42)$$

where

$$C_h = \min \left(\frac{f_m h_0}{250}, 1 \right) \quad (43)$$

f_m is the nominal centre frequency of a frequency band;

h_0 is the greatest of two heights of the diffraction edge in relation to each of the two mean ground planes source side and receiver side;

λ is the wavelength at the nominal centre frequency of the frequency band considered;

δ is the path difference between the diffracted path and the direct path (see Subsection 1.4.2.3);

C'' is a coefficient used to take into account multiple diffractions:

$C'' = 1$ for a single diffraction.

For a multiple diffraction, if e is the total distance between the diffraction closest to the source and the diffraction closest to the receiver (see Figure 9) and if e exceeds 0.3 m (otherwise $C'' = 1$), this coefficient is defined by:

$$C'' = \frac{1 + (5\lambda/e)^2}{1/3 + (5\lambda/e)^2} \quad (44)$$

The values of Δ_{dif} shall be bound:

- If $\Delta L_d < 0$: $\Delta L_d = 0$ dB
- If $\Delta L_d > 25$: $\Delta L_d = 25$ dB for a diffraction on a horizontal edge and only on the term ΔL_d

The path difference δ is calculated in a vertical plane containing the source and the receiver. This is an approximation in relation to the Fermat principle. The approximation remains applicable here (source lines). The path difference δ is calculated as per definition of the elementary paths defined in Appendix C based on the situations encountered. Several examples are provided in Figure 9. Note: For each configuration, the expression of δ is given.

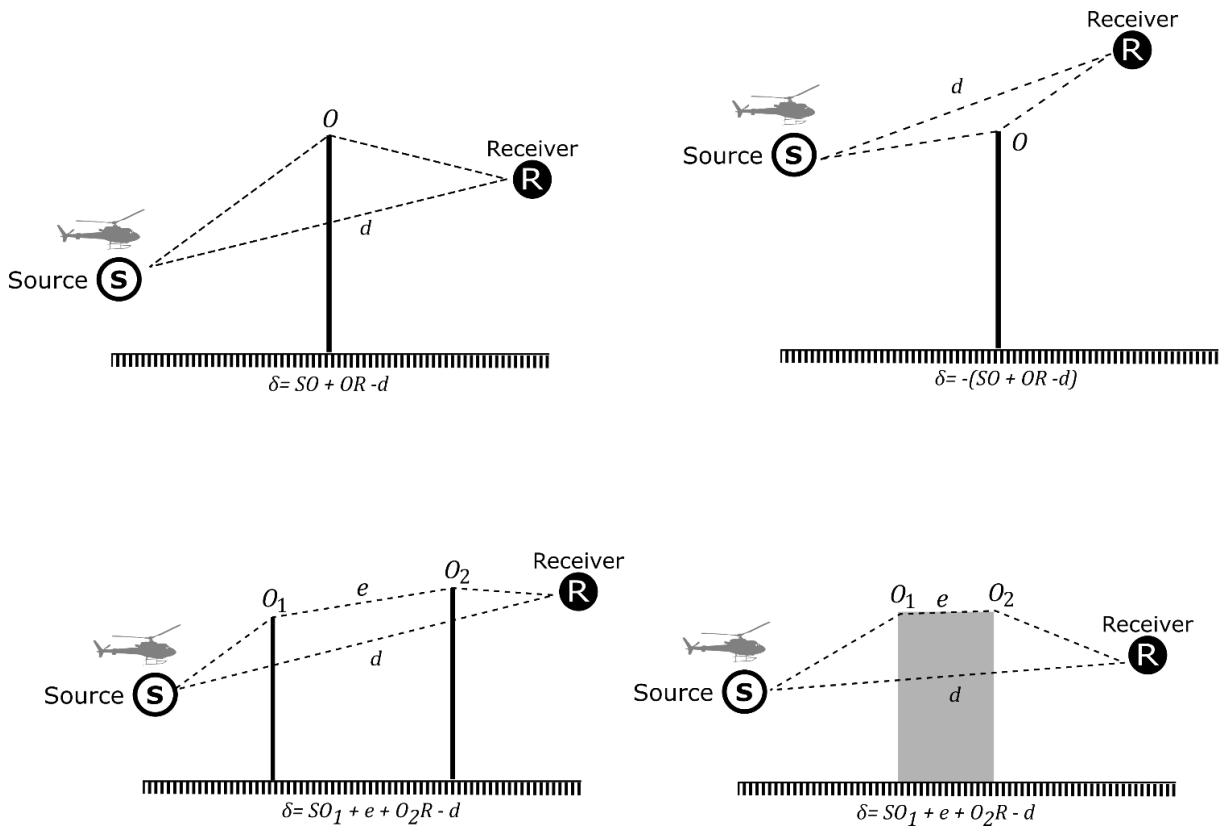


Figure 9 Examples of calculation of the path difference. O , O_1 and O_2 are the diffraction points.

The attenuation due to diffraction and ground absorption $\Delta L_d + \Delta L_g$, taking the ground effects on the source side and receiver side into account, is calculated according to the following general equations:

$$\Delta L_d + \Delta L_g = \Delta L_{d,s} + \Delta L_{g,s} + \Delta L_{g,r} \quad (45)$$

where

$\Delta L_{d,s}$ is the attenuation due to the diffraction between the source S and the receiver R ;

$\Delta L_{g,s}$ is the attenuation due to the ground effect on the source side, weighted by the diffraction on the source side (eq. 46);

$\Delta L_{g,r}$ is the attenuation due to the ground effect on the receiver side, weighted by the diffraction on the receiver side (eq. 47)

In case of multiple diffractions it is understood that $O = O_1$ for calculation of ground attenuation on the source side and $O = O_n$ on the receiver side.

The term $\Delta L_{g,s}$ is given by

$$\Delta L_{g,s} = -20 \log_{10} \left(1 + \left(10^{\frac{-A_{g,s}}{20}} - 1 \right) \cdot 10^{-\frac{(\Delta L_{g,s'} - \Delta L_{d,s})}{20}} \right) \quad (46)$$

$A_{g,s}$ is the attenuation due to the ground effect between the source S and the diffraction point O . This term is calculated with the following hypotheses:

$Z_r = Z_{o,s}$;

$\bar{\sigma}$ is calculated between S and O ;

by the method described in section A.4.4;

$\Delta L_{d,s'}$ is the attenuation due to the diffraction between the image source S' and R , calculated as per eq. 44;

$\Delta L_{d,s}$ is the attenuation due to the diffraction between S and R , calculated as per eq. 44;

The term $\Delta L_{g,r}$ is given by

$$\Delta L_{g,r} = -20 \log_{10} \left(1 + \left(10^{\frac{-A_{ground(O,R)}}{20}} - 1 \right) \cdot 10^{-\frac{(\Delta L_{d,r'} - \Delta L_{d,s})}{20}} \right) \quad (47)$$

$A_{g,r}$ is the attenuation due to the ground effect between the diffraction point O and the receiver R . This term is calculated with the following hypotheses:

$Z_s = Z_{o,r}$;

$\bar{\sigma}$ is calculated between O and R ;

by the method described in section A.4.4;

$\Delta L_{d,r'}$ is the attenuation due to the diffraction between the source S and the image receiver R' , calculated as in eq. 44;

$\Delta L_{d,s}$ is the attenuation due to the diffraction between S and R , calculated as in Subsection eq. 44.

A.5 Noise calculation

A.5.1 Single event

For a single event and a given observer position, the 1/3 octave band noise levels as function of recorded time shall be calculated by equation 1. From this any required time integrated metric may be calculated.

A.5.2 Multiple events

For the calculation of cumulative noise levels, refer to ECAC Doc 29, Vol.2, chapter 5.

A.5.3 Noise contours

For the calculation of noise contours, refer to ECAC Doc 29, Vol.2, chapter 6.

Appendix A. Noise hemisphere format

This appendix presents the format of noise hemispheres used in the NORAH and HELENA (HELicopter Environmental Noise Analysis tool) models. The structure of a hemisphere file is given below:

[TITLE]

```
17 ! #      Table constants
POLDIST    60 ! Distance at which hemisphere is defined
FREEFIELD  2 ! Atmospheric absorption included in hemisphere
NOVALUE    -999 ! no value indicator
TAMB       298.1      ! Ambient temperature, deg Kelvin
RELHUM     70.0      ! Relative humidity, %
PAMB       101325.0   ! Ambient pressure, Pa
Tm         16.5      ! Measurement ambient temperature at 10m, deg Celsius
RHm        73.2      ! Measurement relative humidity at 10m, %
Pm         101079.2   ! Measurement ambient pressure at 10m, Pa
RmOmega    102.6     ! RotorRPM, rpm
ACSPEED    49.9      ! Indicated airspeed, kts
GAMM       -7.0     ! Path angle, deg
PITCH      -6.8     ! Pitch, deg
ROLL       3.4      ! Roll, deg
TW         5.2      ! Total wind, kts
CW         4.6      ! Cross wind, kts
HW         2.4      ! Head wind, kts
2 ! Number of axis
THETAOBSAC 19 0 3 0
           0 10 20 30 40 50 60 70 80 90 100 110 120 130 140 150 160 170 180
PHIOBSAC 19 0 3 0
          -90 -80 -70 -60 -50 -40 -30 -20 -10 0 10 20 30 40 50 60 70 80 90
0 ! NPARAD: Additional point dependent
parameters
NFREQ      31
```

10 12.5 16 20 25 31.5 40 50 63 80 100 125 160 200 250 315 400 500 630 800 1000 1250 1600 2000 2500
3150 4000 5000 6300 8000 10000

PHIOBSAC= 0.000

.... (DATABLOCK)

where the data block contains the 1/3 octave band hemisphere data as function of polar angle (THETAOBSAC) for the given PHIOBSAC. When no data was collected for a given data bin, the default value -999 is set. The first six table constants define the hemisphere reference distance (POLDIST), the content of the hemisphere (FREEFIELD), the no-value indicator (NOVALUE) and the hemisphere atmospheric conditions (TAMB, RELHUM and PAMB). The other nine parameters record the average conditions (over multiple runs) at which the hemisphere data was acquired. The metadata included in the merged hemisphere file are:

- Tm: Measurement ambient temperature at 10m, deg Celsius
- RHm: Measurement relative humidity at 10m, %
- Pm: Measurement ambient pressure at 10m, Pa
- RmOmega: Rotor RPM, %
- ACSPEED: Indicated airspeed, kts
- GAMM: Path angle, deg
- PITCH: Pitch, deg
- ROLL: Roll, deg
- TW: Total wind, kts
- CW: Cross wind, kts
- HW: Head wind, kts

Appendix B. Numerical evaluation of erf

The error function in the boundary loss factor is evaluated numerically. According to Abramowitz and Stegun¹ (p.328) for $d_R > 3.9$ or $d_X > 3$,

$$(1) \quad e^{-d^2} \operatorname{erfc}(-id) = id \left(\frac{0.4613135}{d^2 - 0.1901635} + \frac{0.09999216}{d^2 - 1.7844927} + \frac{0.002883894}{d^2 - 5.5253437} \right)$$

with an absolute error of less than 2×10^{-6} . When $d_R > 6$ or $d_X > 6$,

$$(2) \quad e^{-d^2} \operatorname{erfc}(-id) = id \left(\frac{0.5124242}{d^2 - 0.2752551} + \frac{0.05176536}{d^2 - 2.724745} \right)$$

with an absolute error of less than 1×10^{-6} . For smaller values of d_R and d_X we resort to a formula by Matta and Reichel²:

$$(3) \quad e^{-d^2} \operatorname{erfc}(-id) = K_1(d_X, d_R) + iK_2(d_X, d_R)$$

with

$$(4) \quad K_1 = \frac{hd_X}{\pi(d_X^2 + d_R^2)} + \frac{2hd_X}{\pi} \sum_{n=1}^{\infty} \frac{e^{-n^2 h^2} (d_X^2 + d_R^2 + n^2 h^2)}{(d_X^2 - d_R^2 + n^2 h^2)^2 + 4d_X^2 d_R^2} - \frac{d_X}{\pi} E(h) \\ + P \text{ if } d_X < \frac{\pi}{h}, \\ + \frac{P}{2} \text{ if } d_X = \frac{\pi}{h} \\ + 0 \text{ if } d_X > \frac{\pi}{h}$$

$$(5) \quad K_2 = \frac{hd_R}{\pi(d_X^2 + d_R^2)} + \frac{2hd_R}{\pi} \sum_{n=1}^{\infty} \frac{e^{-n^2 h^2} (d_X^2 + d_R^2 - n^2 h^2)}{(d_X^2 - d_R^2 + n^2 h^2)^2 + 4d_X^2 d_R^2} + \frac{d_R}{\pi} E(h) \\ - Q \text{ if } d_X < \frac{\pi}{h}, \\ - \frac{Q}{2} \text{ if } d_X = \frac{\pi}{h} \\ + 0 \text{ if } d_X > \frac{\pi}{h}$$

where

$$(6) \quad P = 2e^{-\left(d_R^2 + \frac{2d_X\pi}{h} - d_X^2\right)} \left[\frac{(A_1 C_1 - B_1 D_1)}{(C_1^2 + D_1^2)} \right]$$

$$(7) \quad Q = 2e^{-\left(d_R^2 + \frac{2d_X\pi}{h} - d_X^2\right)} \left[\frac{(A_1 D_1 - B_1 C_1)}{(C_1^2 + D_1^2)} \right]$$

in which

¹ M. Abramowitz and I.A. Stegun (1972), "Handbook of mathematical functions with formula's, Graphs, and mathematical tables", Dover publications, inc., New York

² F. Matta and A.R. Reichel (1971), "Uniform computation of the error function and other related functions", Mathematics of Computation, 25, p.339-344

$$\begin{aligned} A_1 &= \cos(2d_R d_X) \\ B_1 &= \sin(2d_R d_X) \\ (8) \quad C_1 &= e^{-2d_X \pi/h} - \cos(2d_R \pi/h) \\ D_1 &= \sin(2d_R \pi/h) \end{aligned}$$

By setting $h = 0.8$, the error $E(h)$ is less than 10^{-6} and generally the first five terms of the infinite series are sufficient to ensure the required accuracy.

Appendix C. Noise paths

By default, the method calculates sound levels without taking the last reflection from a building façade into account for a receiver close to a façade. To meet the application requirements of the regulations in force in terms of noise thresholds, receivers should generally be placed 2 m in front of building façades. The façade effect, if required to be taken into account, can then be approximated either by (i) adding a pre-defined correction of + 3 dB(A) to the $L_{Aeq,T}$ calculated or (ii) adding a more precise correction as a function of the frequency and site characteristics. Noise propagation paths may be categorized in elementary propagation paths as follows below.

Type 1 paths are 'direct' paths from the source to the receiver, which are straight paths in plane view and which may nevertheless include diffractions on the horizontal edges of obstacles (see Figure 10). These are the easiest scenarios to deal with.

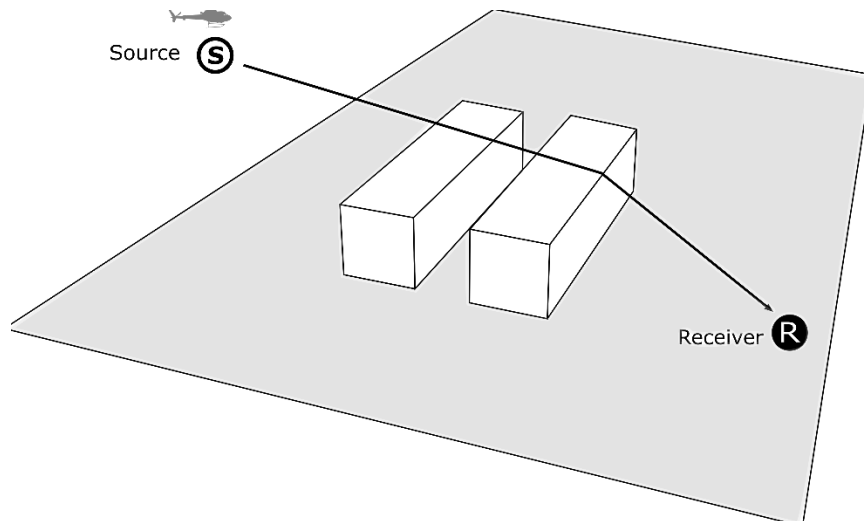


Figure 10 Type 1 path

The 2D section of the geometry is created in a vertical plane passing through the identified path.

Type 2 paths are those that are reflected on vertical or slightly sloping ($< 15^\circ$) obstacles, as shown in Figure 11, which may also include diffractions on the horizontal edges of obstacles (see Figure 12).

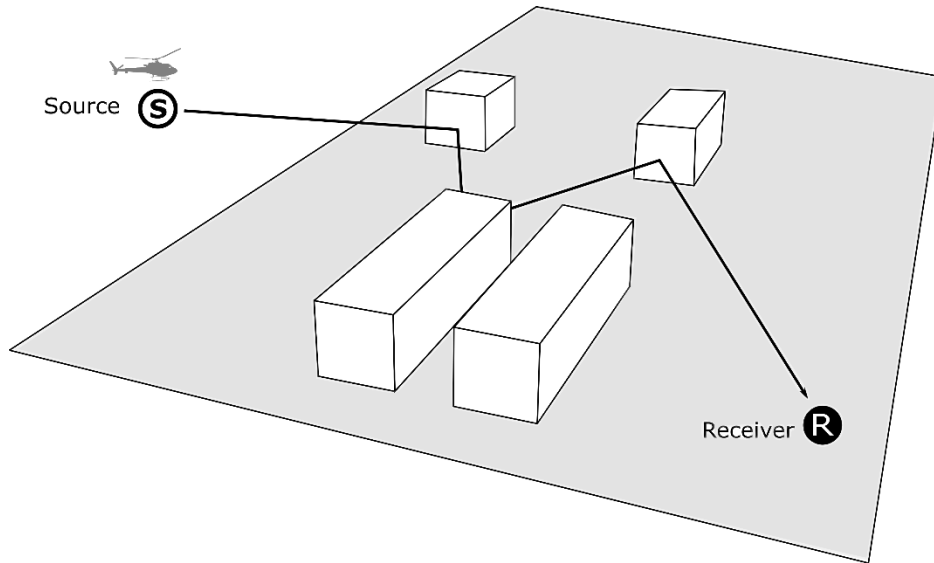


Figure 11 Type 2 path

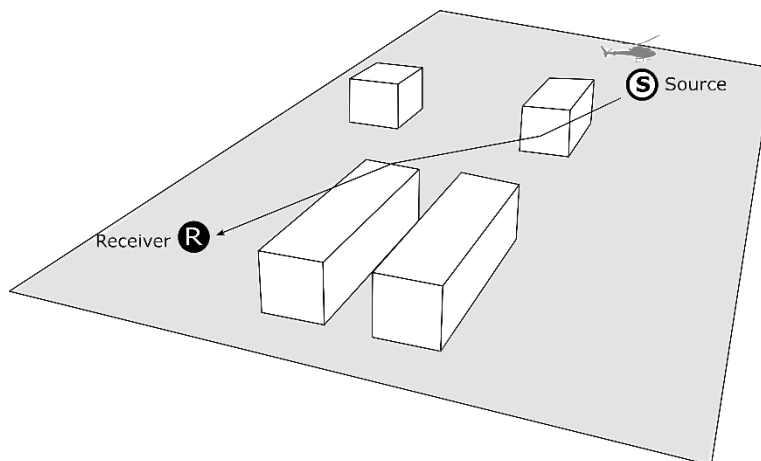


Figure 12 Type 2 path with diffraction on horizontal edge

The principle is to apply the image method. A 2D section of the geometry is created in a succession of vertical planes passing through the straight segments located between two reflections. The section is obtained by unfolding these planes, which resemble a Japanese screen, and the reflections are taken into account by allocating the sound power of a term which takes into account the reflection coefficient of each vertical surface encountered.

Type 3 paths are the paths diffracted by the lateral edges of obstacles (see Figure 13).

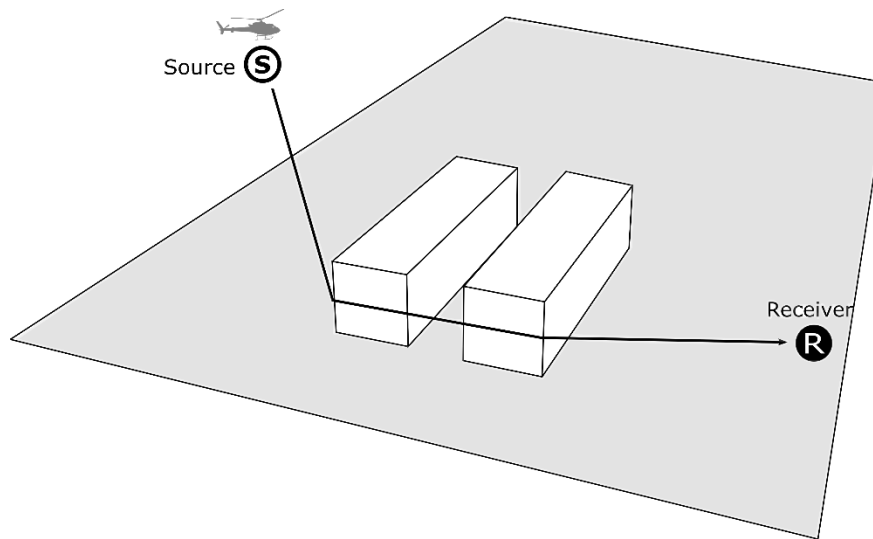


Figure 13 Type 3 path

The principle is to determine each term of Equation (21):

- The term $\Delta L_{d,s}$ is obtained by calculating the path difference δ between the direct path and the convex-hull path of lateral edges in the horizontal plane;
- the term A_g is determined full diffracted sound path (S to R), without taking the presence of the shield into account.

Type 4 paths (Figure 14) are mixed paths which are diffracted by the lateral edges of obstacles and reflected by vertical surfaces ($< 15^\circ$). The calculation is therefore the same as for type 3 paths with a simple correction of the source power as for type 2 paths.

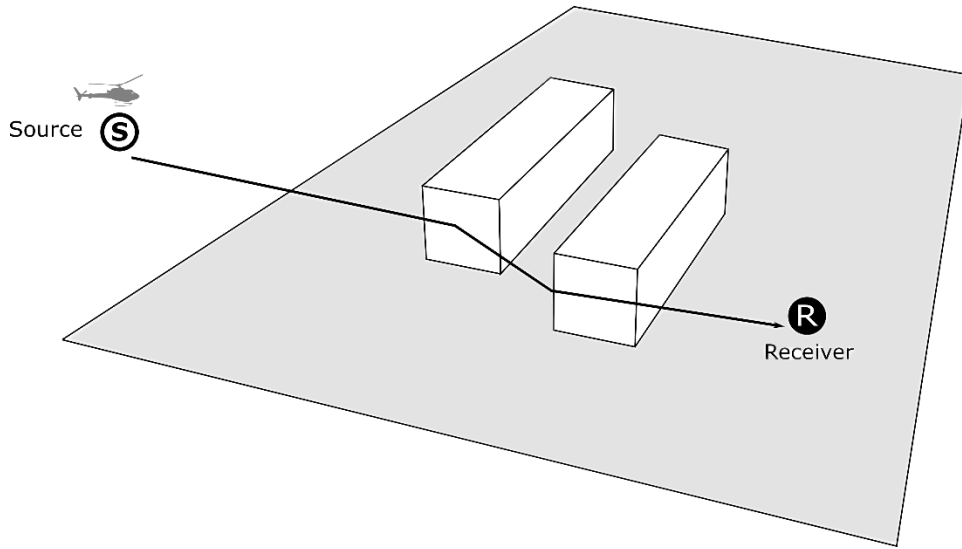


Figure 14 Type 4 paths

Appendix D. Diffraction effects in varying topography

The method for diffraction effects described in this report is limited to screening effects. When applied to varying topography, the method is also limited to consider the vertical plane that contains the source and receiver point. By this limitation, potential lateral diffractions from terrain are ignored. This is no problem because vertical "corners" very seldom occur in nature. Additionally, averaging noise immission over the horizontal spread of source points in normal helicopter movements tends to even out deviations from lateral diffraction.

Topography height information is normally available as *Digital Elevation Models* (see https://en.wikipedia.org/wiki/Digital_elevation_model). Most European countries have data covering the whole country in a regular grid giving the terrain height in evenly spread points. These are typically derived from digital topographical maps or high-resolution measurements from airplanes using Lidar instrumentation. Beside this, terrain elevation models in form of grid- or triangle surfaces can be created by most of the modern GIS systems.

For the helicopter noise calculations, we assume that the user has access to a digital elevation model (DEM) for the calculation task. For each combination of source and receiver point, a vertical relief shall be extracted from the DEM, representing the variation of terrain height across the vertical plane including the two end points. The resolution of the terrain relief shall reflect the resolution of the DEM. If for instance the DEM is a regular grid with 10 m cell size, it is natural to get the terrain height every 10 m along the relief, with every height being interpolated bi-linearly from the closest DEM points. Note that the described algorithms (for instance for the *Mean Plane*) do not require regular spacing between the points. They can be given with arbitrary spacing. But it is a requirement that there is a positive horizontal distance between neighbour points in the relief.

Constructed objects like buildings and screens obviously add diffraction points to the relief when they interfere with the vertical plane between source and receiver. They will act as obstacles that potentially end up as active diffraction points. However, note that constructed objects shall not be included in any topography relief used to calculate *Mean Planes*. The reason is that buildings and noise screens are not assumed to contribute to the ground effect. They only contribute to diffractions and reflections.

Natural screening can occur from any terrain shape that block the line of sight between a source and a receiver. The algorithm for calculating diffraction also include some attenuation in case of negative obstacle heights (negative path length difference). Note that this part for the algorithm applies to points in the relief that are positively identified as potential diffraction points. We recommend that any constructed element that rise more than 0.2 m above the terrain automatically qualify as a potential diffraction point. Natural terrain points which origins from a DEM, however, should not be automatically identified as diffraction points. The reason is a clear risk of accidental screening effects even in flat terrain, in many cases. To avoid, this we recommend a rule that only terrain points which are above the line of sight shall be treated as

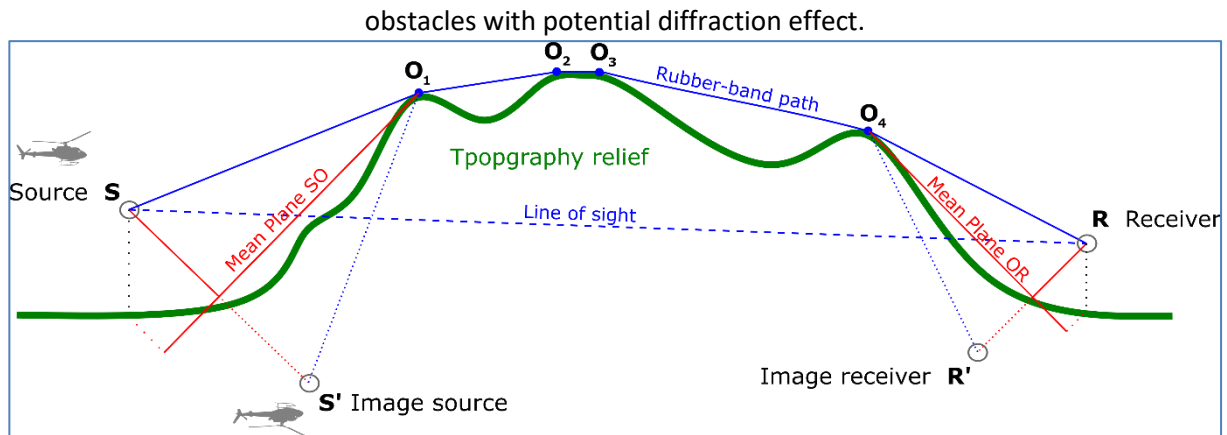


Figure 15 Example of multiple obstacles (O_1 , to O_4) in varying topography

The method description in this report is to some large extent based on Cnossos-EU, because central parts of diffraction algorithms are taken from this common European method for road and railway noise. When considering diffractions, Cnossos EU has focus on urban environments, and does not clearly address how to handle pure topographical diffraction.

We have therefore made figure 15 as an example to clarify handling of multiple obstacles caused by topography. As indicated, the diffracted sound path shall follow a rubber-band line (solid blue) which is the shortest convex-shaped path from the source to the receiver. Every point in the terrain relief (solid green) that is touched by the rubber-band, is a diffracting obstacle. The first and the last obstacle are the most important because they determine partial ground effect related to the diffraction. The remaining obstacles in between contribute to the length of the sound path, used in the diffraction algorithm.

As also indicated (solid red), source side ground effect on diffraction shall base on a *Mean Plane* from the source to the first obstacle. Similarly, receiver side ground effect on diffraction shall use a *Mean Plane* from last obstacle to receiver.

Appendix E. References

- [1.] ECAC, 'Report on Standard Method of Computing Noise Contours around Civil Airports', ECAC Doc29, 4th Ed., 2016
- [2.] M. Tuinstra, N. van Oosten and H. Olsen, 'The development of a European helicopter noise model', 44th European Rotorcraft forum, ERF-2018-50, 2018
- [3.] Rotorspot Rotorcraft Registrations Database; <http://www.rotorspot.nl>
- [4.] Aircraft Type Designators; ICAO Doc 8643, Edition 43; 14 April 2015; <http://www.icao.int/publications/DOC8643/Pages/default.aspx>
- [5.] Jane's All the World's Aircraft; Jane's Information Group.
- [6.] Various manufacturer's brochures, websites, etc.
- [7.] EASA Type Certificate Data Sheets (TCDS); <http://easa.europa.eu/document-library/type-certificates>
- [8.] FAA Type Certificate Data Sheets (TCDS); http://www.airweb.faa.gov/Regulatory_and_Guidance_Library/rgMakeModel.nsf/MainFrame?
- [9.] EASA Noise Type Certificates Rotorcraft, Issue 21; 26 June 2015; <https://easa.europa.eu/document-library/noise-type-certificates-approved-noise-levels>
- [10.] Luftfahrt-Bundesamt (German Federal Aviation Office) Noise Data, List 3: Helicopters; 15 June 2006; <http://www.eacott.com.au/gallery/d/2060-1/Noise+Data+for+Helicopters.pdf>
- [11.] Canadian JHSAT Report 2000 accident data analysis; Canadian Joint Helicopter Safety Analysis Team Year 2000 Summary Report & Flight Hour Data Analysis; <http://www.ihst.org/LinkClick.aspx?fileticket=5OAxM%2fS9lgE%3d&tabid=1507>
- [12.] M.Gervais, V. Gareton, A. Dummel and R. Heger, 'Validation of EC130 and EC135 environmental impact assessment using HELENA', American helicopter soc., 66th annual forum, Phoenix, 2010
- [13.] J.A. Page, C. Wilmer, T. Schultz, K.J. Plotkin and J. Czech, 'Advanced Acoustic Model Technical Reference and User Manual', 2009
- [14.] F. Guntzer, P. Spiegel and M. Lummer, 'Genetic optimization of EC-135 noise abatement flight procedures using an aeroacoustic database', 35th European rotorcraft forum, 2009
- [15.] DOC 9501, Environmental technical manual on the use of procedures in the noise certification of aircraft, 3rd edition, 2004
- [16.] M.Tuinstra, P.Sijtsma, 'Measurement of helicopter noise hemispheres utilizing a 100m vertical array', European Rotorcraft Forum 2012, Amsterdam, ERF-2012-019, 2012
- [17.] R.W. Browne; Munt, R.M.; Simpson, C.R.; Williams, T.; Prediction of Helicopter Noise Contours for Land Use Planning, AIAA Paper 2004-2811, Manchester, UK, 2004
- [18.] F.H. Schmitz and Y.H. Yu, 'Helicopter Impulsive Noise: Theoretical and Experimental Status', NASA TM 84390, 1984
- [19.] SAE, 'Application of pure-tone atmospheric absorption losses to one-third octave-band data', ARP5534, 2013

- [20.] E.J. Rickley, G.G. Flemming, C.J. Roof, 'Simplified procedure for computing the absorption of sound by the atmosphere', *Noise Control Eng. J.*, Vol. 55, No.6, pp482-494, 2007
- [21.] C.F. Chien and W.W. Soroka (1980), 'A note on the calculation of sound propagating along an impedance plane', *J. Sound Vib.*, 69:340-343
- [22.] C.F. Chien and W.W. Soroka (1976), 'Sound propagation along an impedance plane', *J. Sound Vib.*, 43:9-20
- [23.] X. Di and E. Gilbert (1993), 'An exact Laplace transform formulation for a point source above a ground surface', *J. Acoust. Soc. Am.*, 93, 714-720
- [24.] L.C. Sutherland and G.A. Daigle (1997), 'Encyclopedia of acoustics', chapter 32, pp341-365, ISBN 0-471-80465-7
- [25.] M. Abramowitz and I.A. Stegun (1972), 'Handbook of mathematical functions with formula's, Graphs, and mathematical tables', Dover publications, inc., New York
- [26.] F. Matta and A.R. Reichel (1971), 'Uniform computation of the error function and other related functions', *Mathematics of Computation*, 25, p.339-344
- [27.] M.E. Delaney and E.N. Bazley (1970), 'Acoustic properties of fibrous absorbent materials', *Appl. Acoust.*, Vol. 3, pp.105-116
- [28.] N. van Oosten, L. Meliveo, M. Tuinstra, H. Olsen, 'The new EU helicopter noise model NORAH', 11th European Congress and Exposition on Noise Control Engineering, Euronoise, 2018
- [29.] E. N. J. O. J. E. U. L. Directive, "Commission Directive (EU) 2015/996 of 19 May 2015 establishing common noise assessment methods according to directive 2002/49/ec of the European Parliament and of the Council," 2015.
- [30.] S. Kephelopoulos, M. Paviotti, and F. J. C. n. a. m. i. E. Anfosso-Lédée, "Common noise assessment methods in Europe (CNOSSOS-EU)," ed: Publications Office of the European Union, 2012.



European Union Aviation Safety Agency

Konrad-Adenauer-Ufer 3
50668 Cologne
Germany

Project website <https://www.easa.europa.eu/research-projects/environmental-research-rotorcraft-noise>

Tel. +49 221 89990- 000
Mail research@easa.europa.eu
Web www.easa.europa.eu

An Agency of the European Union

